Use of a 3D Inkjet-Printed Model to Access Dust Particle Toxicology in the Human Alveolar Barrier

Dayoon Kang
Pohang University of Science and Technology
Hyomin Lee
Pohang University of Science and Technology
Sungjune Jung (sjjung@postech.ac.kr)
Pohang University of Science and Technology

Research Article

Keywords: 3D alveolar barrier, Inkjet bioprinting, Dust particle toxicity, Inflammation, Pulmonary disease, A2 fine test dust

Posted Date: February 3rd, 2022

DOI: https://doi.org/10.21203/rs.3.rs-1305886/v1

Abstract

Background: Fine dust particles in the air travel into our body via the airway tract and cause severe respiratory diseases. Thus, the analysis of the effects of dust particles on the respiratory system has been receiving significant research interest. However, most studies on the toxicity of dust particles involve two-dimensional (2D) cell cultures, animal models, and epidemiology. Here, we inkjet-printed an three-dimensional (3D) alveolar barrier model to study how dust particles cause respiratory diseases. The three-layered in vitro model was exposed to A2 fine test dust with varying concentrations and exposure durations.

Results: The results highlighted the destruction of the tissue architecture along with apoptosis in the bioprinted alveolar barrier. The damage at the cellular level induced an increase in the amount of pro-inflammatory cytokines secreted, followed by triggering of the signal transduction pathway and activation of transcription factors. As a consequence of the release of cytokines, the extracellular matrix was degraded, which led to the collapse of the cell structure, loss of cell polarity, and a decrease in the barrier tightness. Further, the pulmonary surfactant protein-related genes in the dust-treated alveolar tissue were investigated to evaluate the possible role of dust particles in pulmonary surfactant dysfunction.

Conclusions: This study demonstrated the use of 3D-printed tissue model to evaluate the physiological impact of fine dust particles on cytotoxicity, alveolar barrier rigidity, and surfactant secretion of an alveolar barrier.

Introduction

Due to accelerated urbanization and modernization, the air quality is deteriorating at an alarming rate, and the detrimental impact on human health is becoming a major source of concern. Decades of epidemiological studies have identified a significant correlation between air pollutants and respiratory diseases and have provided direct evidence that high concentrations of particulate matter in the atmosphere can increase morbidity and mortality [1,2]. Fine dust particles, in particular, are considered the primary cause of serious respiratory diseases as these fine dust particles enter through the respiratory system into the lung during an exchange of oxygen and carbon dioxide. After inhalation and deposition in the lungs, the fine dust particles can infiltrate the pulmonary surfactant and, eventually, the epithelial cells *via* the airway and alveoli, where they are released into the systemic circulatory system, causing damage to cells and tissues [3]. These ambient air pollutants are known to cause acute lung diseases with severe symptoms and aggravating factors, such as decreased lung function, respiratory system inflammation, chronic obstructive pneumonia, asthma, and even lung cancer [4].

The incidence of these diseases has been mainly identified in epidemiological clinical analysis and animal studies. Epidemiologically, the concentration of fine dust particles in confined areas has been measured over the years, and its association with the incidence of lung cancer in the local residents of

the confined areas has been investigated [5]. After controlling most of the potential variables in the enclosed areas, suggestive evidence of a positive correlation between particulate matter exposure and lung cancer was established. Sogl et al. investigated the exposure-response relationship between silica and lung cancer risk using data from the German uranium miner cohort study [6]. The cohort includes 58,677 workers between 1946 and 2003, with individual information on occupational exposure to silica and the potential confounders such as radon and arsenic. Consequently, the study confirmed a positive relationship between silica and lung cancer, particularly for high exposures.

Meanwhile, an increase in lymphocytes, macrophages, and inflammatory cytokines were confirmed in mice exposed to these particles [7]. Inflammatory cytokine activation has been observed in patients with asthma, chronic obstructive pulmonary disease, and pulmonary inflammation, suggesting that continuous exposure to dust particles can increase the susceptibility to these conditions. He et al. identified the allergic inflammatory response mechanism of urban $PM_{2.5}$, or fine inhalable particles with diameters that are generally 2.5 μm or smaller, which is known to exacerbate asthma [8]. This study demonstrated that urban $PM_{2.5}$ may exacerbate allergic inflammation in the murine lung via a TLR2/TLR4/MyD88-signaling pathway. The results suggested that inhalation of urban $PM_{2.5}$ imposes a significant risk for inflammatory and allergic lung diseases. Furthermore, over the decades, the risk of dust particles has been examined by cellular biological analysis, which has been improved to assess the detrimental effects of particles from microscopic and systematic perspectives. Representatively, particulate matter has been demonstrated to aggravate the factors that induce asthma through the growth factor-related signaling pathways of oxidative stress and expression in cultured human bronchial epithelial cells exposed to air [9]. Thus, treatment with growth-factor-receptor antagonist drugs has been proposed to suppress the secretion of asthma-causing substances. Leclercq et al. were studied oxidative, inflammatory, and apoptotic in human lung epithelial cells exposed to air pollution-derived $PM_{2.5}$ and concluded $PM_{2.5}$ can cause cytoplasmic reactive oxygen species overproduction, causing oxidative damage and activating oxygen-sensitive NF-kB signaling pathways, as well as continuous mitochondrial dysfunction that lowers cell energy supply [10].

As stated previously, there are numerous studies on the toxicity of dust particles on epidemiological investigation, 2D cell culture, and animal models; however, based on available information, no relevant study has been conducted involving 3D alveolar tissue models containing multiple layers. The 3D *in vitro* tissue model based on cells originating from humans can provide more in-depth information on the cell–cell and cell–ECM interactions in the *in vivo* environment. Since almost all cells in the *in vivo* environment are surrounded three-dimensionally by other cells and ECMs, 3D cell cultures are more appropriate considering the natural microenvironment of cells [11]. Therefore, 3D artificial tissue possess significant potential for application in translational studies and is expected to bridge the gap between cell cultures and animal models [12]. Meanwhile, bioprinting is a rapidly emerging technology used for creating these 3D culture models. With bioprinting, the simultaneous positioning of biomaterials and living cells in a prescribed layer-by-layer stacking arrangement can be achieved to afford engineered tissues and organs [13,14]. Our recent study demonstrated that the three-layered alveolar barrier model created by inkjet-

bioprinting exhibited the physiological functions of the natural human alveolar barrier [15]. Since inkjet bioprinting can precisely position cells with a high resolution [16–18], it is suitable for mimicking extremely thin and fine structures, such as the alveoli. The tissue produced by the automated integrated inkjet bioprinting system is acceptable for use as a test model for toxicological testing of substances with the capability of quality controlled tissue production.

Here, the detrimental effect of fine dust particles was investigated using an alveolar barrier model fabricated by inkjet printing following the process developed in a previous study. After exposing the fine dust particles to the 3D alveolar barrier, various detailed evaluations associated with respiratory function were performed including tissue metabolism and apoptosis assays, tissue structure changes and barrier integrity verification, and gene analysis. Consequently, physiological and pathological structural changes and gene-level regulation were observed in the tissue exposed to the particles. The results of these studies suggest the correlations between fine dust particles and respiratory diseases.

Results

Exposure of the alveolar barrier construct to dust

The hazard of atmospheric fine dust particles was evaluated using all-inkjet-printed alveolar barrier constructed. On a permeable membrane, endothelial cells, type-I collagen, fibroblast-containing collagen, and types I and II alveolar epithelial cells were sequentially deposited by a high-resolution drop-on-demand inkjet printer that could generate picolitre cell-laden droplets at a high frequency (Figure 1a). The printed models had a three-layered structure with a thickness of approximately 10 μm and consisted of an endothelium, a basement membrane, and an epithelium (Figure 1b). They were cultured for 7 days with the epithelium exposed to air for tissue maturation. After maturation, the epithelium of the tissues was exposed to various concentrations of fine dust particles (0, 30, 100, or 300 μg/cm^2), and was further cultured for 1, 3, 5, or 7 days for analysis (Figure 1c).

Changes in the metabolic activity and barrier functions induced by dust particles

To verify the harmful influence of dust particles on tissue proliferation, a CCK-8 assay was performed at each time point (Figure 2a). The results showed that the tissues and control group treated with 30 μg/cm^2 of dust particles demonstrated almost identical proliferations from day 1 to 7. The proliferation rate of the tissues exposed to 100 and 300 μg/cm^2 of dust particles gradually decreased from day 3, and a value approximately 50% lower than that in the control group was observed on day 7. This result does not indicate the absolute number of dead cells in the tissues; however, it reflects that the dust particles had an adverse effect on the metabolic activity of the tissues.

The changes in alveolar barrier functions were investigated by measuring the electrical resistance of an alveolar barrier (Figures 2b). At all time points, the tissues exposed to 30 μg/cm^2 of dust particles did not show any significant change in the TEER, similar to the control group result. The five-day exposure to

particles for 100 and 300 μg/cm^2 groups resulted in a significant reduction in the barrier resistance. Tissue permeability tests were also conducted by measuring the FITC-dextran fluorescence from the basolateral chamber. Similar to the case in the TEER measurements, the significantly increased permeability to 4 kDa FITC-dextran was observed for 100 or 300 μg/cm^2 groups from day 5 (Figure 2c).

To observe the apoptosis in the dust-treated alveolar barrier constructs, a TUNEL assay was conducted (Figure 3). The TUNEL staining results showed that the exposure of a dust concentration of 100 μg/cm^2 or more led to more apoptotic cells as the dust-exposure duration increased. With the apoptosis, changes in tissue structure were observed. While the three-layer structure of the tissue was maintained until day 7 for the control and 30 μg/cm^2 groups, the basement membranes of 100 and 300 μg/cm^2 groups were decomposed and their boundary between the epithelium and endothelium was not distinguished.

Basement-membrane degradation and surfactant dysfunctions in the dust-treated tissues

Immunohistochemically analysis was performed to demonstrate the structural composition of the basement membrane in the three-layer tissue barriers at 7 days after exposure to fine dust. We investigated the distribution of laminin in the basement membrane whose degradation was confirmed by the TUNEL assay (Figure 4a). Laminin is a major component of basement membrane and is involved in cell adhesion, differentiation and control of cell functions in ECM. Generally, the deposition of laminins indicates the endothelial and epithelial cells aligned at the basement membrane with polarity. In the tissues exposed to dust, laminin accumulation and typical alignment along the epithelium and endothelium were not observed. The laminins synthesized by some cells attached to the degraded ECM, which remained unstable, were detected; however, the polarity of the cells in the tissue was not maintained. Furthermore, to determine the other components of the basement membrane ECM, immunostaining of collagen IV was performed (Figure 4b). Resultantly, a homogeneous distribution of collagen IV in the basement membrane was not observed in the tissues exposed to dust. Collagen IV was unevenly distributed in the tissues treated with dust particles of 100 μg/cm^2 or more, although the overall fluorescence intensity did not decrease. Finally, the surfactant-secretion function of the ATII cells in the epithelium was investigated by Alcian blue staining (Figure 4c). This distinguishable epithelium revealed that the secreted pulmonary surfactant stained in light blue was aligned along with the epithelial cells. For the tissue exposed to 300 μg/cm^2 of dust, only the dust particles administered on the epithelium were stained blue, and there was no part observed in the similar morphology of the stained surfactant.

Effect of dust on the expression of mRNAs in the alveolar barrier constructs

The mRNA expression level was investigated through quantitative PCR (qPCR) to identify the basement membrane breakdown and pulmonary dysfunction in the tissue caused by the fine dust particles. Genes that express pro-inflammatory cytokine (IL-1β and TNFα), matrix metalloproteinase (MMP-1 and MMP-9), integrin subunits α1 and β1 (ITGA1 and ITGB1), and pulmonary surfactant proteins (SP-A and SP-B) were selected. Transcriptomes were analyzed at all time points in the control group and all experimental groups. First, pro-inflammatory cytokines and MMPs were investigated, which are important molecules

produced by the dust particle-simulated tissue and digest ECMs and modulate the degradation of the basement membrane. Overall, the expression levels increased as the fine dust concentration and administration time increased. Specifically, the mRNA level of IL-1β showed a significant increase at day 7 in the 300 μg/cm^2 dust-treated alveolar barrier. The expression level of TNFα was significantly increased in a concentration-dependent manner within the same dust-exposure period (Figure 5b). The effect of the fine dust particles on the expression level of MMP-1 was analyzed, also known as collagenase. The result showed a remarkable increase in the MMP-1 mRNA levels after the tissues were exposed to 300 μg/cm^2 of dust particles for 7 days (Figure 5c). In addition, the expression level of MMP-9, which digests collagen IV substrates, was investigated. The expression level of MMP-9 increased significantly concentration-dependently from day 3 onwards. For the tissue exposed to the highest concentration of dust for the longest time, a remarkable increase in the MMP-9 expression level was confirmed (Figure 5d). It was demonstrated that dust particles contribute to the high expression level of the enzyme that causes ECM turnover and structural changes.

In contrast, the mRNA expression levels of integrins and surfactant proteins were decreased as the fine dust concentration and exposure time decreased. ITGA1 and ITGB1, which encode integrin subunits α1 and β1, are transmembrane receptors that promote cell–cell or cell–ECM adhesion and activate signaling pathways that mediate various cellular signals. The expression level of ITGA1 showed a significant down-regulation from day 3 in the tissues exposed to the highest concentration of dust particles (Figure 5e). In particular, in the tissue exposed to fine dust for seven days, the expression level of ITGA1 significantly reduced, regardless of the dust concentration. Further, the expression level of IGTB1 decreased as the concentration of dust increased, although the decrease was insignificant (Figure 5f). Lastly, the expression levels of hydrophilic SP-A and hydrophobic SP-B were determined, which represent the pulmonary surfactants in the alveoli. Marked differences were noted among the control and experimental groups, with the lowest gene expression levels observed in the dust-exposed tissues. The SP-A expression level in the tissue exposed to 300 μg/cm^2 of dust was significantly decreased from day 1 compared to the control group. A significant decrease was observed in the control group and in the tissues exposed to 100 μg/cm^2 or more of dust particles on day 7 (Figure 5g). The expression level of SP-B was lower in all tissues exposed to dust from day 1 to 7 (Figure 5h). Thus, dust particles inhibit the secretion of respiratory surfactants in alveolar tissues and have the potential to cause surfactant-related physiological dysfunction.

Discussion

The use of 3D *in vitro* tissue constructs in toxicology has been increasing over the last decade as a new preclinical testing platform and as an alternative to animal testing. In this study, we introduced a 3D *in vitro* alveolar barrier model to evaluate the harmful effects of fine dust particles. Our findings demonstrated that the all-inkjet-printed alveolar barrier model closely mimics the morphological, functional, and micro-environmental features of the human alveolar tissue and could be a successful testing platform to evaluate the disease-inducing effects of inhalable particles potential for toxicology.

Lung epithelial cells are the first site of entry for atmospheric particles and infectious organisms from the external environment and provide early signals for the inflammatory response via the release of pro-inflammatory cytokines and inflammatory mediators. Pro-inflammatory cytokines, which are critical to the initiation of an inflammatory response, trigger the signal transduction pathway, leading to the activation of transcription factors. This affects a variety of genes involved in numerous biological processes, such as cell survival, apoptosis, and diseases [19]. The expression level of pro-inflammatory cytokines was increased in dust exposed tissues (Figures 5a and b). Generally, the release of pro-inflammatory cytokines leads to tight junction degradation and loss of barrier integrity [20,21]. Tight junctions are known to play a role in trapping airborne particulate matter and removing it from the respiratory tract, and particulate matter-induced damage is a major cause of epithelial barrier disruption in lung inflammation [22]. As high concentrations of dust particles induced upregulation of pro-inflammatory cytokine expression, barrier resistance decreased and permeability increased, indicating a loss of epithelial junctional function (Figures 2b and c). Additionally, we identified the expression levels of laminin and collagen IV, which are major components of the basement membrane ECM, through immunohistochemical analysis and proved that the collapse of the structure is related to the decomposition of the basement membrane (Figures 4a and b).

MMPs are the major enzymes involved in ECM degradation and the cleavage of ECM components with broad substrate specificity. Normally, the activity of MMPs is low; however, the activity increases during repair or remodeling and in diseased tissues, inflamed tissue, and tissues exposed to air pollutants [23,24]. MMP-induced ECM breakdown contributes significantly to the progression of several lung pathologies, including cancer and epithelial–mesenchymal transition [25,26]. The upregulation of MMP along with the secretion of pro-inflammatory cytokines was observed (Figures 5c and d), and it is known that the upregulation of MMPs is mediated by the secretion of pro-inflammatory cytokines, such as IL-1β and TNFα [27]. Additionally, the integrins function as receptors for cell–cell and cell–ECM adhesion, and they affect the orientation of the intracellular actin cytoskeleton, which induced by the integrin interactions is essential for the cell polarity signals that define the position of the basal domain [28,29]. Cells require polarity to establish their barrier function, and cell polarity is essential for cell migration in the correct direction, creating distinct leading and trailing structures [30]. Loss of cell polarity and tissue disorganization are the hallmarks of cancer and tumor initiation [31]. The upregulation of MMPs and loss of the barrier integrity, induced by the pro-inflammatory cytokines, have been employed as markers of respiratory diseases [32–34]. In this study, the expression level of integrin receptors decreased with an increase in MMP and degradation of the ECM (Figures 5e and f). Thus, the exposure to particulate matter may be responsible for the initiation of lung inflammation and the development of lung cancer.

Finally, the effects of dust particles on the secretion of the pulmonary surfactant were investigated. This surfactant is essential for breathing as it lines the alveoli to reduce surface tension, thereby preventing atelectasis. In the tissues exposed to dust particles, the reduction of pulmonary surfactant expression was observed (Figures 5g and h). Malformation in surfactant production or function is associated with several pulmonary diseases, simultaneously, and pulmonary inflammation changes the surfactant metabolism. Representatively, the deficiency of surfactants has been linked to a variety of diseases, such

as respiratory distress syndrome, idiopathic pulmonary fibrosis, and asthma [35]. The all-inkjet-printed alveolar barrier exhibits the risk potential of fine dust particles to induce severe respiratory diseases, such as fibrosis and asthma.

The one limitation of this study is the exclusion of alveolar macrophages in the all-inkjet-printed alveolar barrier constructs. Generally, alveolar macrophages account for 9.4% of cells in the human alveoli [36]. Inhaled particles can modify immune function by directly affecting antigen-presenting macrophages, thus upregulating the normal lymphocytic response to antigens in the lung [37]. To simulate and implement the immune system and disease induction that occur in the human body, further investigations are required using artificial alveoli that include immune cells. If this limitation is overcome in future works and the alveolar barrier contains immune cells, this method has the potential to pave the way for investigations of the toxicity of inhaled particles and the associated respiratory diseases.

Conclusion

In summary, the analysis of all-inkjet-printed alveolar barrier constructs afforded three major new insights regarding the harmful effects of inhaled dust particles. The phenomena in the alveolar tissue exposed to high concentrations of fine dust particles include the following: (i) an increased expression of pro-inflammatory cytokines, (ii) destruction and disorganization of tissue architecture, and (iii) up- or downregulation of genes associated with respiratory diseases. The findings of this study suggest that the *in vitro* artificial tissue structure created using bioprinting technology can be used as an innovative testing platform to evaluate the disease-inducing effects of inhalable particles. Products fabricated using bioprinting can be customized by introducing complexity or patient-specificity into the system, as required, to meet the requirements of users. Therefore, it is expected to be used in various fields. In addition, since some of the phenomena occurring in the body are mimicked, the fundamental understanding of the infection process will be improved, and tests for toxic substances and antigens will be accelerated. The all-inkjet-printed alveolar barrier model is capable of simulating the physiological phenomena in the body with a high degree of accuracy. This suggests that it can be used as a preclinical model in toxicology and facilitate the translation of new findings into effective treatment strategies.

Materials And Methods

Cell culture

The alveolar epithelial cell lines (NCI-H1703 (ATCC, VA, USA) and NCI-H441 (ATCC)) were cultured in a complete cell-growth medium, (RPMI-1640 (HyClone, UT, USA)) supplemented with 10% fetal bovine serum (FBS; HyClone) and a 1% antibiotic/antimycotic solution (HyClone). Lung fibroblasts (MRC5 (ATCC)) were cultured in MEM α (HyClone) with 10% FBS and a 1% antibiotic/antimycotic solution. Lung microvascular endothelial cells (HULEC-5a (ATCC)) were cultured in the MCDB 131 medium (Thermo Fisher Scientific, MA, USA) supplemented with 10 mM l-glutamine (Sigma-Aldrich, MO, USA), 1 µg/mL hydrocortisone (Sigma-Aldrich), 10 ng/mL human EGF recombinant protein (Thermo Fisher Scientific),

10% FBS, and a 1% antibiotic/antimycotic solution. All cell types were cultured at 37 °C in a humidified atmosphere containing 5% CO_2. The cells were subcultured upon growth to a sufficient level of confluence.

Engineering and 3D culture of the alveolar barrier

The alveolar barrier construct was fabricated by printing the four different cell types in a layer-by-layer manner using the drop-on-demand inkjet bioprinting system (Jetlab II; MicroFab, TX, USA). The total numbers of printed NCI-H1703, NCI-H441, MRC5, and HULEC-5a cells were 8×10^4, 1.6×10^5, 1.8×10^5, and 3×10^5, respectively, which was consistent with the numbers of cells in the natural human alveoli [36]. The all-inkjet-printed alveolar barrier was cultured in a 1:1:1 mixture of the complementary cell-culture medium (RPMI-1640, MEM α, and MCDB 131) with aprotinin (100 Kallikrein inhibitor unit) (A1153, Sigma-Aldrich). The growth medium (500 µL) was added to the basolateral side of the 12-mm cell culture insert, whereas the apical side was exposed to air during the incubation. The culture medium was replaced once a day. The cells were cultured at 37 °C in a humidified atmosphere of 5% CO_2 for 7 days before the dust-particle assessment. The information on detailed fabrication process can be described elsewhere [15].

Dust preparation and tissue exposure

As model fine dust particles, Arizona A2 fine test dust (ISO 12103-1, Powder Tech. Inc., MN, USA) was used which consists of 69-77% quartz. The particles were stirred in Dulbecco's phosphate-buffered saline (DPBS, HyClone) at concentrations of 67.2, 224, and 672 µg/mL, after which they were vortexed for a few seconds before use. After 7 days of air exposure, the alveolar barrier constructs were treated with dust particles at concentrations of 30, 100, and 300 µg/cm^2 in DPBS. To determine the concentration of dust particles per unit area, 500 µL of the solution was administered to the tissue epithelial layer over an area of 1.12 cm^2. The epithelial layer of the control group was immersed in a 500 µL DPBS solution without dust. The dust-particle-exposure durations were 1, 3, 5, and 7 days. Over time, the dust particles settled in the epithelial layer.

Tissue proliferation assay

Tissue proliferation and metabolic activity were assessed in the dust-treated alveolar barrier constructs using Cell Counting Kit 8 (CCK 8; Dojindo Laboratories, Japan). The assay reagent was mixed with the cell growth medium in the ratio of 1:9. Thereafter, 0.5 mL of the mixture was added to the basolateral side of the 12-mm cell-culture insert and incubated for 1.5 h. The ultraviolet A (UVA) absorbance of the mixture was measured at 450 nm at each time point using a microplate reader (Spark; Tecan, Switzerland).

Measurement of tissue-barrier integrity

Warm (37 °C) DPBS portions (0.5 mL) were added to the apical side and the basolateral chambers (1.5 mL) of the cell culture insert. Thereafter, the alveolar barrier model was incubated for 20 min. The

transepithelial/endothelial electrical resistance (TEER) was measured using an EVOM2 (World Precision Instruments, FL, USA) instrument with double chopstick electrodes (STX2, World Precision Instruments). a rubber O-ring was mounted on the cell culture insert to minimize the effect of contraction of a collagen basement membrane. The cell-free permeable membrane (reference) was also measured for the TEER while the O-ring was attached.

The permeability of the alveolar barrier model was investigated with 70 kDa FITC-dextran (Sigma-Aldrich) as a probe for successful permeability. The alveolar barriers were rinsed gently with Hanks' balanced salt solution (HBSS; Sigma-Aldrich) two times and transferred to another fresh 12-well plate, which was filled with 1.5 mL of HBSS. The HBSS (0.5 mL) containing 1 mg/mL of FITC-dextran was added to the apical side of the cell culture insert and incubated for 1 h. The concentration of the transferred FITC-dextran from the basolateral chamber was determined using a fluorescence multi-well plate reader (Spark; Tecan) with excitation and emission wavelengths of 490 and 520 nm, respectively. A new sample was used at each time point.

Histological analysis

For the histological evaluation of the dust-treated alveolar barrier models, the samples were fixed in 1 mL of a 4% paraformaldehyde solution that was added to the tissue basolateral chamber overnight. The samples containing a porous membrane were cut out from the cell culture insert. The samples were embedded in optimal cutting temperature compounds (Leica Biosystems, Germany) and frozen at −80 °C. Serial 10-μm-thick sections were obtained using a cryostat (CM1860; Leica Biosystems). The tissue sections were stained with hematoxylin (Mayer's; Dako, CA, USA) and eosin Y (0.5% alcohol; Merck, Germany) to visualize and compare the structures of the tissues treated with dust particles. The sections were stained with Alcian blue (pH: 2.5; Sigma-Aldrich) for observation of secreted surfactant, and nuclear fast red (Sigma-Aldrich) stained the cell nuclei.

To determine the effect of the dust-particle treatment on the apoptosis in the alveolar barrier construct, the frozen sections were examined for the presence of apoptotic cells with fragmented DNA by the TdT-mediated dUTP nick-end labeling (TUNEL) assay using a commercially available kit (G3250, Promega, WI, USA), as detailed in the manufacturer's protocol. The cell nuclei were stained with propidium iodide (Sigma-Aldrich).

To observe the existence and degradation of ECM, immunohistochemical analysis was performed on the tissue slices. A blocking solution was prepared by mixing 5% FBS, 3% bovine serum albumin (BSA; Thermo Fisher Scientific), and 0.1% Triton X-100 (Sigma-Aldrich) in PBS. The primary antibodies used in these protocols were rabbit anti-collagen IV (1:200, PA1-28534, Thermo Fisher Scientific) and rabbit anti-laminin (1:200, ab11575, Abcam, Cambridge, UK). The Alexa Fluor® 488-conjugated goat anti-rabbit secondary antibody was used to visualize the targets (1:100, a11034; Thermo Fisher Scientific). The cell nuclei were stained with Hoechst 33342 (1:5000; Sigma-Aldrich). For the histological analysis, all the bright field and fluorescence images were captured by a microscope (Ti-S; Nikon, Japan)

RNA extraction and gene analysis

The tissues were washed with PBS and centrifuged. The total RNA was extracted from pellets using the RNeasy Mini Kit (Qiagen, Germany). Afterward, it was measured quantitatively using an ultraviolet–visible (UV–Vis) spectrophotometer (NanoDrop One, Thermo Fisher Scientific). The extracted RNA was reverse-transcribed using the oligo dT and high-capacity cDNA reverse transcription kit (Applied Biosystems, CA, USA), according to the manufacturer's protocols. Each cDNA was detected using a real-time polymerase chain reaction (PCR) system (StepOne Plus, Applied Biosystems) with the SYBR Green Master Mix (Applied Biosystems). The sequences of the forward and reverse primer pairs are shown in Table S1, Supporting Information. The reference gene, glyceraldehyde 3-phosphate dehydrogenase, was used to normalize the raw C_T (cycle threshold) values.

Statistical analysis

Quantitative data are expressed as means, with error bars representing ± standard error of the mean. One-way analysis of variance (ANOVA) with Tukey test was carried out to determine the statistical significance of the differences between experimental groups using the OriginPro 2016 software (OriginLab, MA, USA). The sample size (n) and preprocessing normalization of data are given in the corresponding figure legends. In all cases, a p-value of <0.05 was considered to reflect significance.

Abbreviations

2D: Two-dimensional; 3D: Three-dimensional; qPCR: Quantitative polymerase chain reaction; MMP: Matrix metalloproteinase; SP: Surfactant protein; ECM: Extracellular matrix; TEER: Transepithelial/endothelial electrical resistance; TUNEL: TdT-mediated dUTP nick-end labelling.

Declarations

Ethics approval and consent to participate

Not applicable.

Consent for publication

Not applicable.

Competing interests

The authors have no competing financial interest to declare.

Acknowledgements

Not applicable.

Authors' contributions

DK: Methodology, Designed and performed the research, Data curation, Conceptualization, Original draft preparation; HL: Conceptualization, Writing-Reviewing and Editing; SJ: Supervision, Conceptualization, Writing-Reviewing and Editing; SJ is a corresponding author. All authors read and approved the final manuscript.

Funding

This work was supported by the National Research Foundation of Korea (NRF) grants funded by the Korean government (2021R1A4A1021972).

Availability of data and materials

The datasets used and/or analyzed during the current study are available from the corresponding author on reasonable request.

References

1. Ibald-Mulli A, Wichmann HE, Kreyling W, Peters A. Epidemiological evidence on health effects of ultrafine particles. J Aerosol Med Depos Clear Eff Lung. 2002;15:189–201.
2. Xing YF, Xu YH, Shi MH, Lian YX. The impact of PM2.5 on the human respiratory system. J Thorac Dis. 2016;8:E69–74.
3. Cho CC, Hsieh WY, Tsai CH, Chen CY, Chang HF, Lin CS. In vitro and in vivo experimental studies of PM 2.5 on disease progression. Int J Environ Res Public Health. 2018;15:1–26.
4. Jiang XQ, Mei XD, Feng D. Air pollution and chronic airway diseases: What should people know and do? J Thorac Dis. 2016;8:E31–40.
5. Consonni D, Carugno M, De Matteis S, Nordio F, Randi G, Bazzano M, et al. Outdoor particulate matter (PM10) exposure and lung cancer risk in the EAGLE study. PLoS One. 2018;13:1–20.
6. Sogl M, Taeger D, Pallapies D, Brüning T, Dufey F, Schnelzer M, et al. Quantitative relationship between silica exposure and lung cancer mortality in German uranium miners, 1946–2003. Br J Cancer. 2012;107:1188–94.
7. Chan YL, Wang B, Chen H, Ho KF, Cao J, Hai G, et al. Pulmonary inflammation induced by low-dose particulate matter exposure in mice. Am J Physiol - Lung Cell Mol Physiol. 2019;317:L424–30.
8. He M, Ichinose T, Yoshida Y, Arashidani K, Yoshida S, Takano H, et al. Urban PM2.5 exacerbates allergic inflammation in the murine lung via a TLR2. Sci Rep. Springer US; 2017;7:1–9.
9. Hyseni X, Soukup JM, Huang YCT. Pollutant particles induce arginase II in human bronchial epithelial cells. J Toxicol Environ Heal - Part A Curr Issues. 2012;75:624–36.
10. Leclercq B, Kluza J, Antherieu S, Sotty J, Alleman LY, Perdrix E, et al. Air pollution-derived PM2.5 impairs mitochondrial function in healthy and chronic obstructive pulmonary diseased human

bronchial epithelial cells. Environ Pollut. Elsevier Ltd; 2018;243:1434–49.
11. Edmondson R, Broglie JJ, Adcock AF, Yang L. Three-dimensional cell culture systems and their applications in drug discovery and cell-based biosensors. Assay Drug Dev Technol. 2014;12:207–18.
12. Jensen C, Teng Y. Is It Time to Start Transitioning From 2D to 3D Cell Culture? Front Mol Biosci. 2020;7:1–15.
13. Moroni L, Burdick JA, Highley C, Lee SJ, Morimoto Y, Takeuchi S, et al. Biofabrication strategies for 3D in vitro models and regenerative medicine. Nat Rev Mater. Springer US; 2018;3:21–37.
14. Sun W, Starly B, Daly AC, Burdick JA, Groll J, Skeldon G, et al. The bioprinting roadmap. Biofabrication. 2020;12:022002.
15. Kang D, Park JA, Kim W, Kim S, Lee H, Kim W, et al. All-Inkjet-Printed 3D Alveolar Barrier Model with Physiologically Relevant Microarchitecture. Adv Sci. 2021;2004990:2004990.
16. Kim YK, Park JA, Yoon WH, Kim J, Jung S. Drop-on-demand inkjet-based cell printing with 30-μm nozzle diameter for cell-level accuracy. Biomicrofluidics. 2016;10.
17. Park JA, Yoon S, Kwon J, Now H, Kim YK, Kim W-J, et al. Freeform micropatterning of living cells into cell culture medium using direct inkjet printing. Sci Rep. Springer US; 2017;7:14610.
18. Yoon S, Park JA, Lee H-R, Yoon WH, Hwang DS, Jung S. Inkjet-Spray Hybrid Printing for 3D Freeform Fabrication of Multilayered Hydrogel Structures. Adv Healthc Mater. 2018;7:1800050.
19. Kataoka T. Chemical biology of inflammatory cytokine signaling. J Antibiot (Tokyo). Nature Publishing Group; 2009;62:655–67.
20. Wang T, Wang L, Moreno-Vinasco L, Lang GD, Siegler JH, Mathew B, et al. Particulate matter air pollution disrupts endothelial cell barrier via calpain-mediated tight junction protein degradation. Part Fibre Toxicol. 2012;9:1–12.
21. Zhang L, Wang C, Xian M, Ma S, Wang K, Lou H, et al. Particulate matter 2.5 causes deficiency in barrier integrity in human nasal epithelial cells. Allergy, Asthma Immunol Res. 2020;12:56–71.
22. Wittekindt OH. Tight junctions in pulmonary epithelia during lung inflammation. Pflugers Arch Eur J Physiol. Pflügers Archiv - European Journal of Physiology; 2017;469:135–47.
23. Bonnans C, Chou J, Werb Z. Remodelling the extracellular matrix in development and disease. Nat Rev Mol Cell Biol. 2014;15:786–801.
24. Dagouassat M, Lanone S, Boczkowski J. Interaction of matrix metalloproteinases with pulmonary pollutants. Eur Respir J. 2012;39:1021–32.
25. Balestrini JL, Niklason LE. Extracellular Matrix as a Driver for Lung Regeneration. Ann Biomed Eng. 2015;43:568–76.
26. Borthwick LA, Parker SM, Brougham KA, Johnson GE, Gorowiec MR, Ward C, et al. Epithelial to mesenchymal transition (EMT) and airway remodelling after human lung transplantation. Thorax. 2009;64:770–7.
27. MANICONE A, MCGUIRE J. Matrix metalloproteinases as modulators of inflammation. Semin Cell Dev Biol. 2008;19:34–41.

28. Giancotti FG. Integrin Signaling. Science. 1999;285:1028–33.
29. Manninen A. Epithelial polarity – Generating and integrating signals from the ECM with integrins. Exp Cell Res. 2015;334:337–49.
30. Campanale JP, Sun TY, Montell DJ. Development and dynamics of cell polarity at a glance. J Cell Sci. 2017;130:1201–7.
31. Lee T-J, Park S, Bhang SH, Yoon J-K, Jo I, Jeong G-J, et al. Graphene enhances the cardiomyogenic differentiation of human embryonic stem cells. Biochem Biophys Res Commun. Elsevier Inc.; 2014;452:174–80.
32. Ostridge K, Williams N, Kim V, Bennett M, Harden S, Welch L, et al. Relationship between pulmonary matrix metalloproteinases and quantitative CT markers of small airways disease and emphysema in COPD. Thorax. 2016;71:126–32.
33. Parks WC, Shapiro SD. Matrix metalloproteinases in lung biology. Respir Res. 2001;2:10–9.
34. Tatsuta M, Kan-O K, Ishii Y, Yamamoto N, Ogawa T, Fukuyama S, et al. Effects of cigarette smoke on barrier function and tight junction proteins in the bronchial epithelium: Protective role of cathelicidin LL-37. Respir Res. Respiratory Research; 2019;20:1–14.
35. Han S, Mallampalli RK. The Role of Surfactant in Lung Disease and Host Defense against Pulmonary Infections. Ann Am Thorac Soc. 2015;12:765–74.
36. Pinkerton KE, Gehr P, Castañeda A, Crapo JD. Architecture and Cellular Composition of the Air–Blood Tissue Barrier. Comp Biol Norm Lung. Elsevier; 2015. p. 105–17.
37. Hamilton RF, Holian A, Morandi MT. A comparison of asbestos and urban particulate matter in the in vitro modification of human alveolar macrophage antigen-presenting cell function. Exp Lung Res. 2004;30:147–6.

Figures

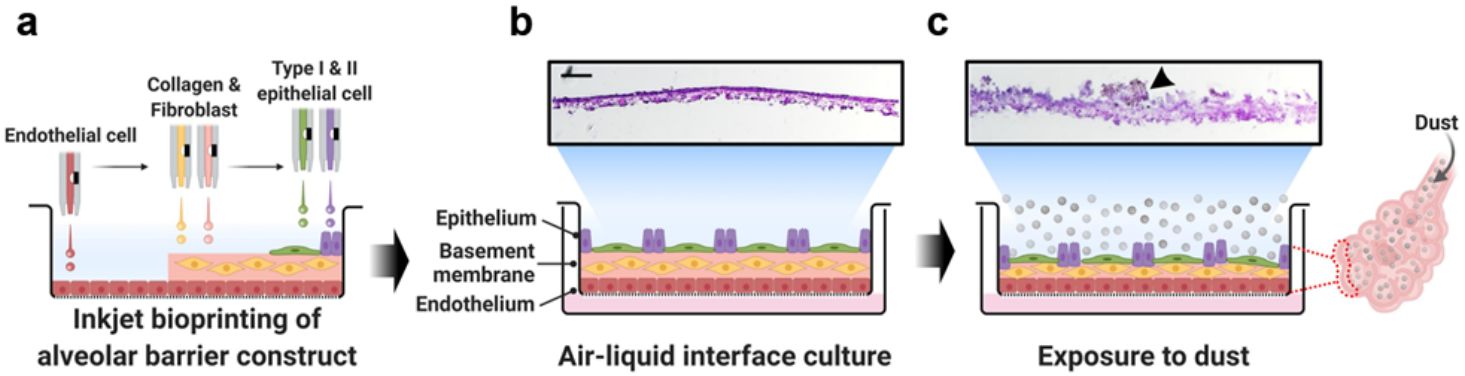

Figure 1

Schematic diagram of the research process. (a) The alveolar barrier constructs fabricated by the sequentially stacking of alveolar microvascular endothelial cells, collagen and lung fibroblasts, and types

□ and □ alveolar epithelial cells using inkjet bioprinting technology. (b) The printed alveolar barrier construct cultured for seven days with the epithelium exposed to air for tissue maturation. (c) Alveolar barrier constructs treated with different concentrations of dust (0–300 μg/cm^2) for different durations (from 1–7 days). A cross-sectional image of the alveolar barrier model stained with hematoxylin & eosin Y. The black arrows indicate the dust particles on the epithelium. Scale bar = 50 μm.

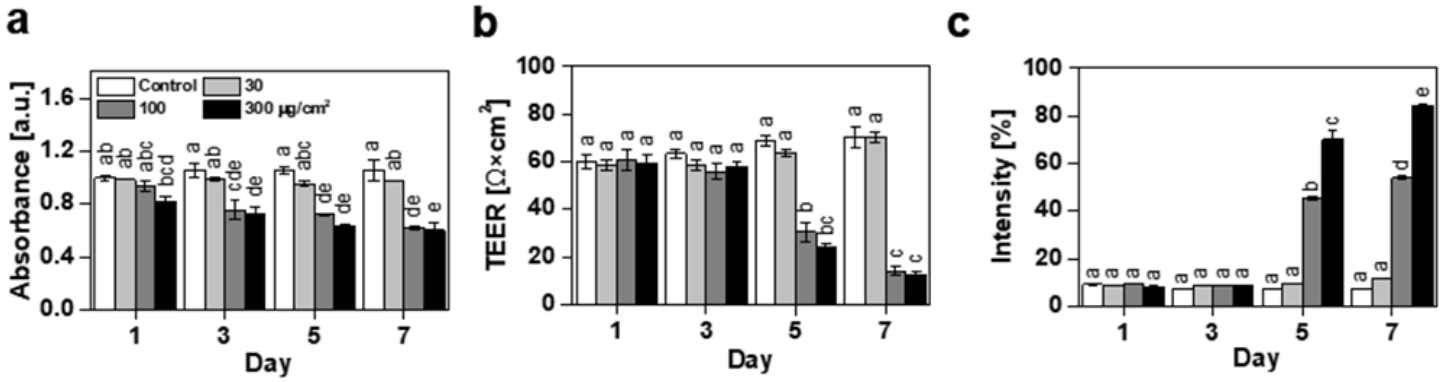

Figure 2

Effects of the dust concentration and exposure times on the viability and properties of the alveolar barrier constructs. (a) *CCK-8 assay was implemented to detect tissue proliferation. Absorbance was normalized using the control group on day 1 (data normalization = 1).* ***(b)*** *TEER was measured to identify the tissue barrier integrity post exposure to dust.* ***(c)*** *Barrier permeability was measured according to the amount of FITC-dextran passing through the tissue barrier. Fluorescence intensity was normalized using the blank as the permeable membrane without cells (data normalization = 100). The different letters indicate significant differences ($p < 0.05$). All data are presented as mean ± standard error of the mean (n = 3).*

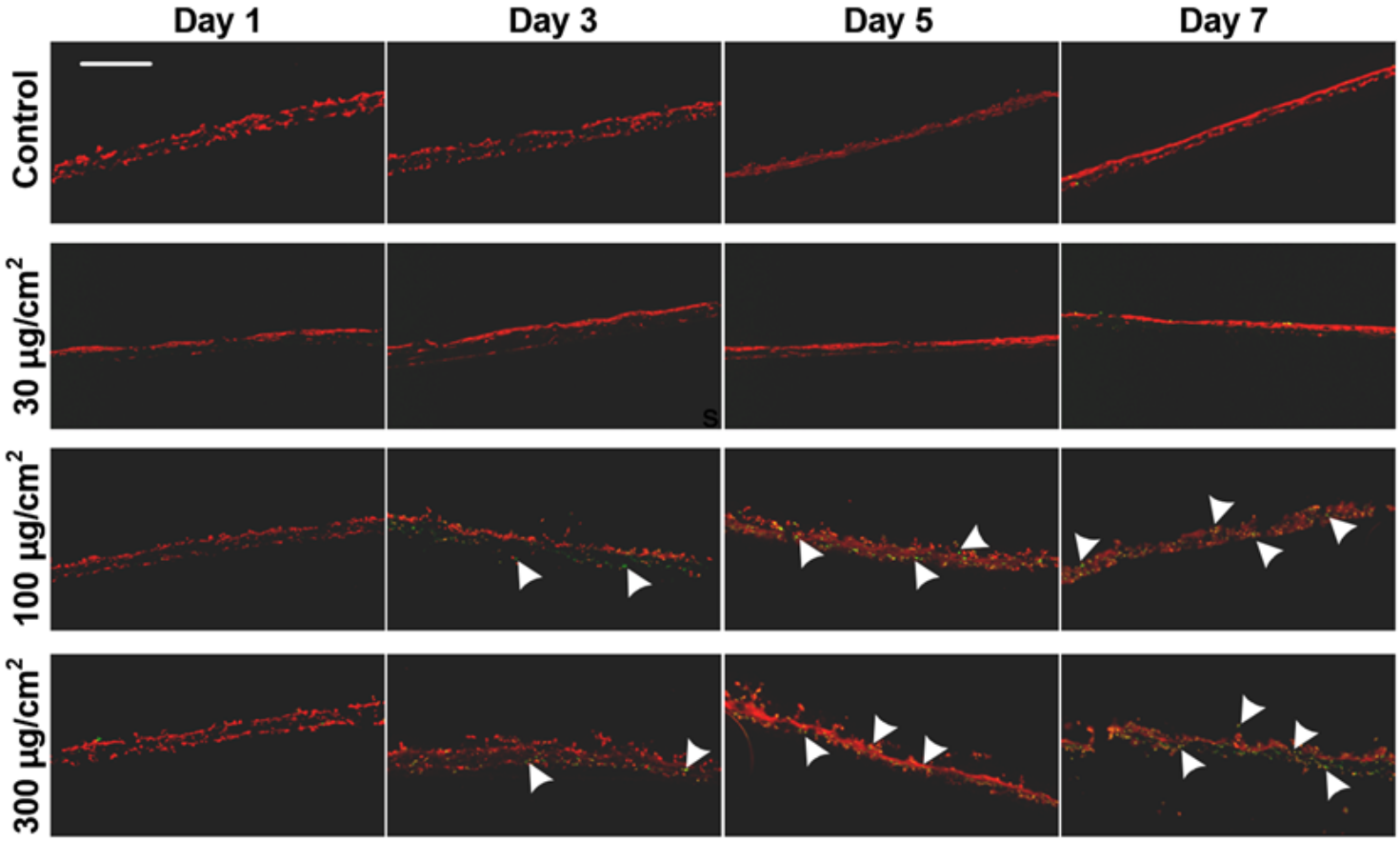

Figure 3

Observation of the barrier collapse and DNA fragmentation in the alveolar barrier constructs after dust exposure. *The three-layered structure collapse because of the concentration- and time-dependent effects of the dust particles. The number of TUNEL-stained (green) apoptotic cells was significantly increased after treatment with high concentrations of dust. The arrows indicate apoptotic cells. The nuclei were counterstained with PI (red). Scale bar = 50 μm.*

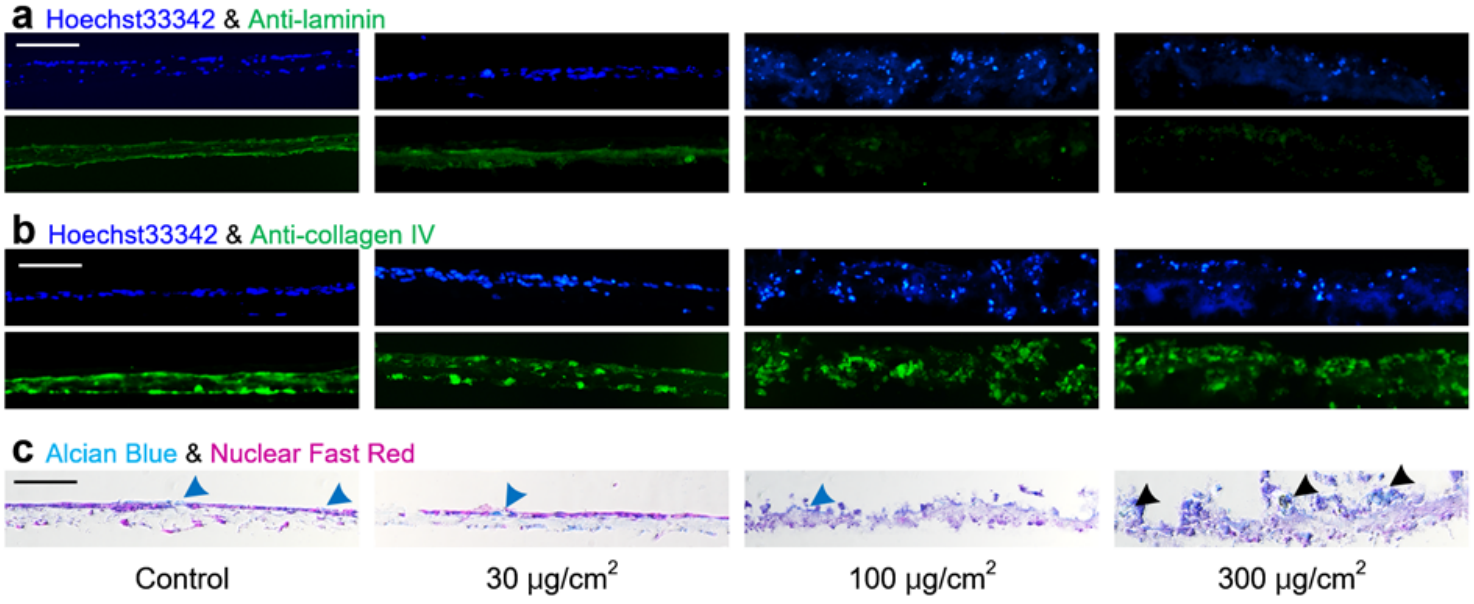

Figure 4

Functional characterization of the alveolar barrier constructs after dust exposure for seven days. (a–b) ***Immunofluorescence microscopic images using specific antibodies (green) and the nuclei staining reagent, Hoechst33342 (blue); the basement membrane constituent*** *(a)* ***laminin and*** *(b)* ***collagen IV.*** *(c)* ***Microscopic cross-sectional image after staining with Alcian blue and nuclear fast red. Nuclei in cells and the secreted surfactant stained in purple and light blue, respectively. The black arrows indicate the dust particles on the epithelium, while the blue arrows indicate the stained surfactant. Scale bar = 50 µm.***

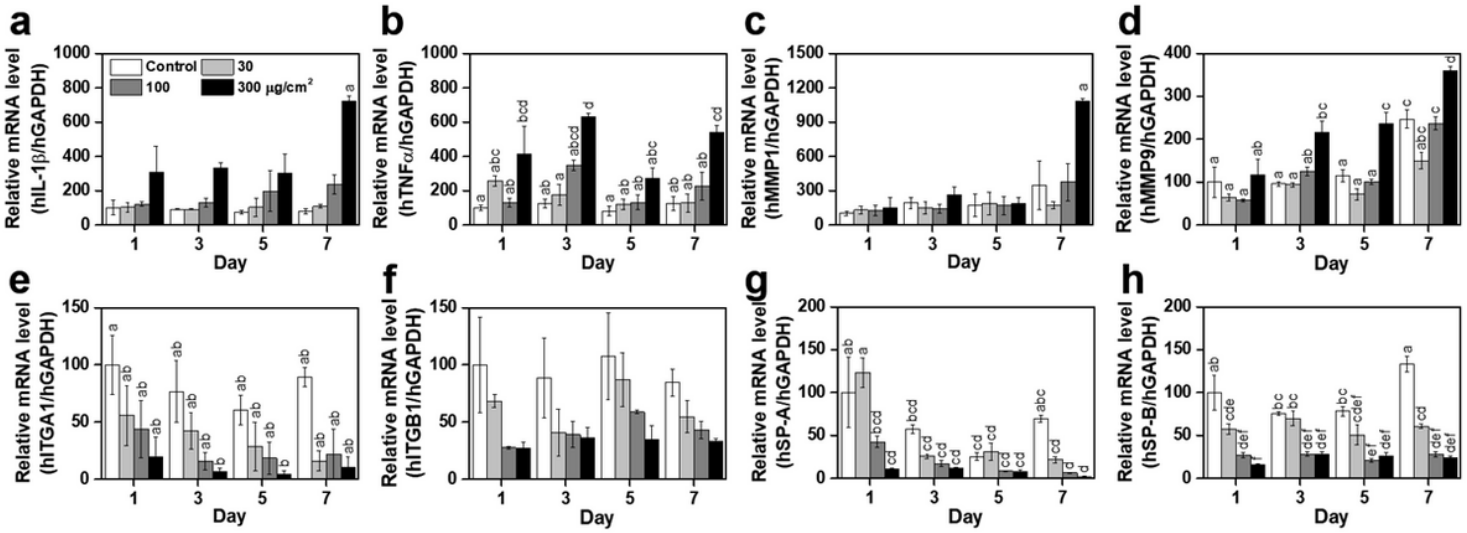

Figure 5

Expression of mRNAs in the alveolar barrier constructs. ***Relative mRNA expression was measured via qPCR using specific markers involved in pro-inflammatory cytokines*** *(a and b)****, metalloproteases*** *(c and d)****, integrin subunits*** *(e and f)****, and pulmonary surfactant protein*** *(g and h)****. The expression level of each gene was normalized using the expression level in the control group on day 1 (data normalization = 100). The different letters indicate the significant differences (p < 0.05). All data are presented as mean ± standard error of the mean (n = 3).***

Supplementary Files

This is a list of supplementary files associated with this preprint. Click to download.

- Supportingdata.docx